ChemComm

COMMUNICATION

View Article Online
View Journal | View Issue

Cite this: *Chem. Commun.*, 2025, **61**, 3732

Received 18th October 2024,
Accepted 26th January 2025

DOI: 10.1039/d4cc05547k

rsc.li/chemcomm

Pseudomorphic replication for surface patterning with porphyrinic metal–organic frameworks†

Nina F. Suremann and Sascha Ott *

An unexplored strategy for controlled surface patterning with porphyrinic metal–organic frameworks (MOFs), integrating atomic layer deposition (ALD) and pseudomorphic replication (PMR), is presented. Surface patterning with a sub-micrometer size resolution is enabled by translating ALD-patterned Al_2O_3 into a MOF pattern in the presence of a porphyrinic linker.

Metal–organic frameworks (MOFs) are composed of metal-based secondary building units (SBUs) that are interconnected by organic linker molecules to form three-dimensional porous structures with high internal surface areas. Due to the modular nature to mix and match SBUs and linkers, MOFs are highly versatile, and have found applications in, for example, gas separation and storage,[1] catalysis,[2–5] and sensing.[6] Opportunities to further exploit the unique properties of MOFs for advanced applications would be enabled by precise patterning of MOFs on specific substrates. In general, the intentional arrangement of surface structures has been shown in the past to allow for customized material design, with applications in electronics, materials science, medicine, and other industries.[7–12] In analogy, assembling MOFs in a defined surface pattern would create precise spatial arrangements to achieve specific function.[13,14] Recognizing this largely untapped potential, MOF patterning has started to attract attention, and various approaches have been described to-date (Fig. 1).[15] Amongst them, top-down approaches start from a homogeneous MOF layer from which specific parts are etched away by, for example, direct X-ray or electron-beam lithography.[16] Other examples include photoacid-induced etching[17] or crosslinking-induced patterning through photo- and electron-beam lithography.[18] In printing approaches, inks from pre-formed MOFs are applied to the substrate in defined patterns.[19] Bottom-up approaches use methods to predefine areas for localized MOF growth, such as seed crystals.[20] MOF surface patterning is however still in its infancy, and the development of novel MOF patterning strategies is clearly motivated.

A hitherto unexplored strategy for surface patterning is the concept of pseudomorphic replication (PMR). Derived from geology, 'pseudomorph' refers to a process where one material retains the structure of another despite having undergone a transformation. What makes PMR particularly interesting is its potential for adaptation and application in the field of chemistry.[21–24] In the context of MOFs, PMR has been explored as a technique to create specific 3D architectures around shape-directing templates,[24,25] opening up possibilities for tailoring the properties of these intriguing materials. In terms of surface patterning on flat substrates, PMR may offer opportunities to grow MOFs from precursors that are deposited at defined positions on a substrate. Atomic layer deposition (ALD) of metal oxides would be ideally suitable for this purpose as this method allows the spatially defined deposition of metal oxides, which may provide the cations for SBU formation and MOF growth. Moreover, ALD is a well-established technique for the precise fabrication of thin films on various surfaces, and is already

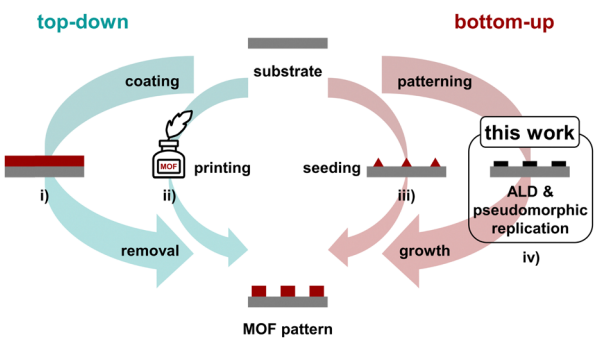

Fig. 1 Schematic representation of different possibilities to create MOF-patterned surfaces with top-down or bottom-up approaches: (i) patterned etching of a homogeneously coated surface,[16–18] (ii) "printing" the pattern with MOF ink,[19] (iii) seeding crystals,[20] and (iv) patterning of a growth-directing reagent applied by atomic layer deposition (ALD), followed by pseudomorphic replication (this work).

Department of Chemistry Ångström Laboratory, Uppsala University, Box 523, 75120 Uppsala, Sweden. E-mail: sascha.ott@kemi.uu.se

† Electronic supplementary information (ESI) available. See DOI: https://doi.org/10.1039/d4cc05547k

utilized in patterning.[26,27] Unlike conventional methods that deposit materials in bulk, ALD operates at an atomic, layer-by-layer scale and allows for meticulous control over the surface pattern of the deposited materials. The opportunity to administer different types of precursors leads to a range of ALD-deposited materials that can potentially be utilized for further processing such as PMR. Furthermore, metal oxide coatings administered by ALD were shown to be translated into MOF layers before.[28,29]

In this work, the possibility of MOF surface patterning based on PMR from a defined metal oxide pattern that was obtained by ALD is investigated. The patterned metal oxide substrate was created with a mask during the ALD process (Experimental and Fig. S1, ESI†). More specifically, spatially separated stripes of Al_2O_3 on silicon substrates were exposed to a porphyrinic linker solution to induce MOF growth through PMR. From the description of PMR as a dissolution and recrystallization process at a solid–liquid interface,[30] three fundamentally different reaction outcomes are plausible. As schematically depicted in Fig. 2, uniform MOF film growth across the entire substrate (outcome (i)) is expected from decoupled dissolution of the metal oxide and MOF formation, thereby losing the spatial information that was introduced during ALD. Outcome (ii) is an intermediate scenario in which the ALD pattern can still be observed, but lacks spatial precision. Finally, outcome (iii) is the desired case, where MOF growth exclusively occurs at the areas that were covered with the metal oxide during ALD. This outcome also implies that the metal oxide may not be fully dissolved, and the cations assemble the SBU before they diffuse away from the substrate. Herein, we show compelling evidence that the micrometer-sized pattern from the ALD can directly be translated into MOF growth with a sub-micrometer size resolution, which is in the same size domain as the size of the MOF crystallite.

A MOF with porphyrinic linkers and Al^{3+}-hydroxo/oxo cluster SBUs that can be constructed from ALD-patterned Al_2O_3 was chosen for this study. Deposited Al_2O_3 has a thickness of 5 nm,

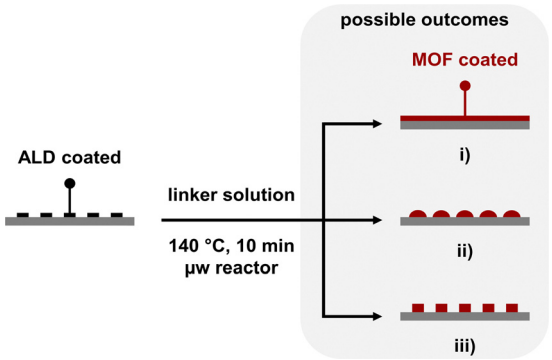

Fig. 2 Schematic representation of patterned MOF growth. A substrate is coated with a metal oxide through atomic layer deposition (ALD), followed by pseudomorphic replication (PMR) to facilitate the transformation into the MOF-coated sample. Three potential outcomes may be expected: (i) complete loss of spatial information, (ii) leakage around the edges of the metal oxide pattern, or (iii) MOF growth only observed where the substrate was covered with metal oxide.

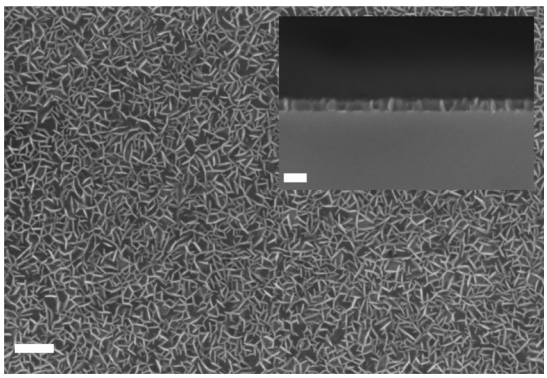

Fig. 3 SEM image of an as-synthesized $Al_2(OH)_2CuTCPP$@Si material. The scale bar indicates 200 nm. Inset: Cross-section SEM image showing a uniform height of the MOF crystallites of 60 nm. The scale bar indicates 100 nm.

as expected from 50 ALD cycles. For the PMR, silicon substrates with deposited Al_2O_3 were subjected to microwave-induced MOF syntheses at 140 °C for 10 min in the presence of the porphyrinic linker CuTCPP (5,10,15,20-tetrakis(4-carboxyphenyl)porphyrin copper(II)) to form the composite material $Al_2(OH)_2CuTCPP$@Si.

In order to assess general MOF growth under these conditions and to characterize the MOF morphology, $Al_2(OH)_2CuTCPP$@Si was first grown on homogeneously Al_2O_3-coated silicon. Scanning electron microscopy (SEM) images revealed homogeneous coverage of the complete surface with platelet-like crystals (Fig. 3), consistent with earlier studies of a related material with Co-porphyrinic linkers.[22] As shown in the inset of Fig. 3, the Al_2O_3 is converted to MOF platelets of *circa* 60 nm height that stand upright on the underlying substrate (Fig. S2, ESI†). The extent of aluminum oxide conversion is assumed to be complete, in analogy to a literature report that described a nearly linear correlation between the Al_2O_3 layer and resulting MOF thickness.[29] The X-ray photoelectron spectroscopy (XPS) survey spectrum (Fig. S6, ESI†) showed signals for Cu 2p and N 1s, with the Cu 2p high-resolution spectrum confirming Cu(II)-typical satellite features (Fig. S7a, ESI†).[31] X-ray diffraction further confirmed the crystallinity of the MOF (Fig. S10, ESI†).

Having established general MOF growth on homogeneously Al_2O_3-coated silicon substrates, the surface patterning was investigated on Al_2O_3-patterned substrates. The success of MOF surface patterning *via* PMR was investigated by comparison of SEM images of the ALD-coated substrate (Fig. 4a–c) with those of the corresponding MOF-coated sample (Fig. 4d–f). Important to note is that all SEM images in Fig. 4 were obtained from one and the same wafer on which the same spot was located for meaningful comparisons. Fig. 4a–c shows SEM images of the Al_2O_3-coated silicon substrate at different magnifications. A pattern of stripes that is created through the mask in the ALD is clearly visible. The white regions of the image arise from the non-conductive Al_2O_3 surface, while the dark parts represent the conductive bare silicon surface, as indicated. Zooming in on the stripes allows the determination of their width to be 33.3 μm (Fig. S3c, ESI†), as well as the identification of small distinct imperfections of the ALD pattern on the 1 μm scale (Fig. 4c). After SEM analysis, the

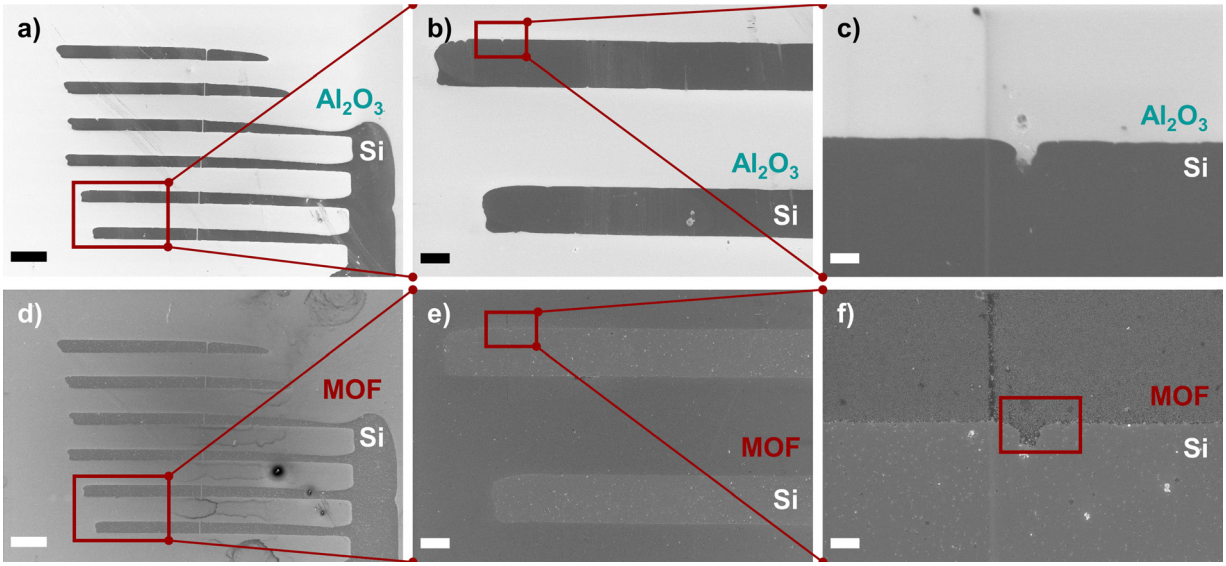

Fig. 4 SEM images of an Al_2O_3@Si substrate (a)–(c) and of the same sample after pseudomorphic MOF synthesis as a MOF@Si material (d)–(f). The scale bars indicate 100 μm (a) and (d), 20 μm (b) and (e), and 2 μm (c) and (f), respectively.

wafer was exposed to the PMR procedure as described above. As expected, the optical contrast between the MOF@Si composite and the Si substrate in the SEM images (Fig. 4d–f) is less prominent than that between the Al_2O_3@Si and Si, because both MOF and Si are conductive.

The observed MOF pattern after PMR is identical to that of the original Al_2O_3 after ALD, proving that the overall pattern is retained during the PMR process. Furthermore, the width of a silicon stripe was measured before and after PMR at three different points resulting in a mean distance of 33.3 μm and 33.4 μm, respectively (Fig. S3c and d, ESI†). Thus, no obvious diffusion of dissolved Al^{3+} from the Al_2O_3 stripes is observed, and the ALD pattern is conserved. The ALD blueprint is directly translated into a MOF pattern as the metal oxide acts as a growth-directing reagent.

To establish the resolution limit that can be achieved with the synergistic ALD/PMR approach, the edges of the pattern were examined more closely (Fig. 4f). At this scale, the individual MOF platelets become clearly visible, in analogy to the observation in Fig. 3. While the MOF–silicon interface is an almost perfectly straight line, reflecting the ALD pattern (Fig. S4, ESI†), even the smallest features are translated from Al_2O_3 into $Al_2(OH)_2$CuTCPP. This is visualized in a distinct shape that was chosen in the ALD-patterned substrate (Fig. 4c and f). A direct comparison of the spot before and after MOF growth highlights the conservation of the shape during PMR (Fig. S5c, ESI†). Zooming in on the detail in Fig. 4f, it is possible to determine its dimensions to be 1.65 μm and 1.47 μm (Fig. S5d, ESI†).[32] These findings show that the ALD blueprint is conserved and translated into the MOF pattern with a sub-micrometer resolution. The Al_2O_3 SBU precursor is acting as a growth-directing reagent and the synthetic PMR clearly follows a concerted dissolution and crystallization mechanism, where the pattern is preserved. For future studies, this means that the size of the MOF crystallites may ultimately determine the resolution limit.

Further validation that the MOF is only grown where Al_2O_3 had been deposited was obtained from XPS analysis with X-ray induced secondary electron imaging (Fig. S8, ESI†). With a beam diameter of 10 μm, it is possible to measure survey spectra specifically of the silicon stripe and the MOF area. Two representative measurements are depicted in Fig. 5 (Fig. S9, ESI†). The spectrum recorded within a silicon area (blue) shows a strong Si 2p signal as well as the typically expected signals for C 1s and O 1s due to contaminations and surface silicon oxides, respectively. This demonstrates that there is indeed no MOF growth on bare silicon where no Al_2O_3 had been deposited by ALD. In contrast, the spectrum recorded within the MOF-overgrown area (red) shows signals for Cu 2p and N 1s that arise from the Cu-porphyrin MOF. The peak in the C 1s region is of higher intensity than that of the Si stripe, and also assigned to the porphyrinic linker. At the same time, the Si 2p signal is completely absent, consistent with XPS being a surface-sensitive method that will not penetrate the sample to sufficient depth to show the underlying silicon substrate.

In summary, it is shown that the spatial accuracy of the ALD process can be retained during PMR, thereby offering a promising approach for controlled bottom-up surface patterning with nm-sized MOF crystals. It is demonstrated that the PMR is confined to the area of the metal oxide, which thus determines the sites of MOF growth. This implies that the metal oxide does not simply dissolve during PMR, but stays preserved within at least a few tens of nm and is translated into the MOF crystallites. The resolution of the ALD/PMR integrated approach is either given by the resolution of the ALD pattern or by the crystallite size of the MOF after PMR, whichever is limiting. This approach holds significant potential for advancing surface patterning techniques, offering a pathway for the patterning of surfaces with different MOF structures for application in, for example, catalytic tandem reactions.

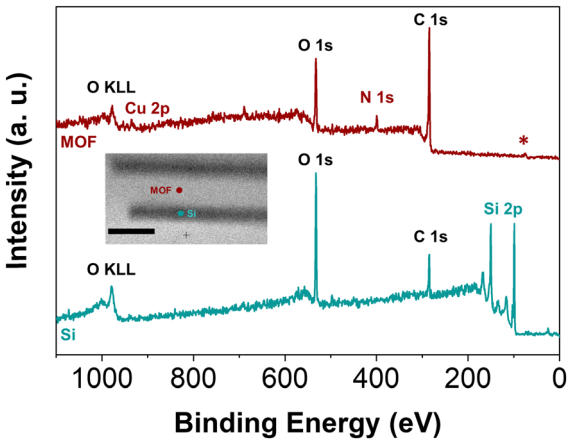

Fig. 5 X-ray photoelectron spectra of an $Al_2(OH)_2CuTCPP$@Si composite within a silicon (blue) or a MOF-overgrown area (red). The asterisk (*) marks overlapping Cu 3p and Al 2p signals. The inset shows the X-ray induced secondary electron image obtained to locate the measurement points. The scale bar indicates 100 μm.

We acknowledge financial support from the Swedish Energy Agency (42029-2) and the Swedish Research Council (2023-03395). We thank Milena Moreira for the fabrication of the 2-photon printed mask. We thank Amol Kumar for the XRD measurements, and acknowledge Myfab Uppsala for providing facilities and experimental support. Myfab is funded by the Swedish Research Council (2020-00207) as a national research infrastructure.

Data availability

The data supporting this article have been included as part of the ESI.† There are additional references within the ESI.† [31–34]

Conflicts of interest

There are no conflicts to declare.

Notes and references

1 H. Li, K. Wang, Y. Sun, C. T. Lollar, J. Li and H.-C. Zhou, *Mater. Today*, 2018, **21**, 108–121.
2 C. Xu, R. Fang, R. Luque, L. Chen and Y. Li, *Coord. Chem. Rev.*, 2019, **388**, 268–292.
3 M. B. Majewski, A. W. Peters, M. R. Wasielewski, J. T. Hupp and O. K. Farha, *ACS Energy Lett.*, 2018, **3**, 598–611.
4 J.-S. Qin, S. Yuan, C. Lollar, J. Pang, A. Alsalme and H.-C. Zhou, *Chem. Commun.*, 2018, **54**, 4231–4249.
5 N. F. Suremann, B. D. McCarthy, W. Gschwind, A. Kumar, B. A. Johnson, L. Hammarström and S. Ott, *Chem. Rev.*, 2023, **123**, 6545–6611.
6 L. E. Kreno, K. Leong, O. K. Farha, M. Allendorf, R. P. Van Duyne and J. T. Hupp, *Chem. Rev.*, 2012, **112**, 1105–1125.
7 Y. Lei, S. Yang, M. Wu and G. Wilde, *Chem. Soc. Rev.*, 2011, **40**, 1247–1258.
8 Z. Nie and E. Kumacheva, *Nat. Mater.*, 2008, **7**, 277–290.
9 D. Wouters and U. S. Schubert, *Angew. Chem., Int. Ed.*, 2004, **43**, 2480–2495.
10 Z. Burton and B. Bhushan, *Nano Lett.*, 2005, **5**, 1607–1613.
11 R. F. Pease and S. Y. Chou, *Proc. IEEE*, 2008, **96**, 248–270.
12 D.-H. Kim, H. Lee, Y. K. Lee, J.-M. Nam and A. Levchenko, *Adv. Mater.*, 2010, **22**, 4551–4566.
13 P. Falcaro, D. Buso, A. J. Hill and C. M. Doherty, *Adv. Mater.*, 2012, **24**, 3153–3168.
14 P. Falcaro, R. Ricco, C. M. Doherty, K. Liang, A. J. Hill and M. J. Styles, *Chem. Soc. Rev.*, 2014, **43**, 5513–5560.
15 C. L. Ruiz-Zambrana, M. Malankowska and J. Coronas, *Dalton Trans.*, 2020, **49**, 15139–15148.
16 M. Tu, B. Xia, D. E. Kravchenko, M. L. Tietze, A. J. Cruz, I. Stassen, T. Hauffman, J. Teyssandier, S. De Feyter, Z. Wang, R. A. Fischer, B. Marmiroli, H. Amenitsch, A. Torvisco, M. D. J. Velásquez-Hernández, P. Falcaro and R. Ameloot, *Nat. Mater.*, 2021, **20**, 93–99.
17 Z. Zhu, F. Li, J. Li, Q. Chen, W. Li, Z. Tang, W. Xu, W. Shen, T. H. Tao, L. Sun, Y. Fu and M. Tu, *ACS Nano*, 2024, **18**, 19628–19635.
18 X. Tian, F. Li, Z. Tang, S. Wang, K. Weng, D. Liu, S. Lu, W. Liu, Z. Fu, W. Li, H. Qiu, M. Tu, H. Zhang and J. Li, *Nat. Commun.*, 2024, **15**, 2920.
19 C.-H. Su, C.-W. Kung, T.-H. Chang, H.-C. Lu, K.-C. Ho and Y.-C. Liao, *J. Mater. Chem. A*, 2016, **4**, 11094–11102.
20 E. Zanchetta, L. Malfatti, R. Ricco, M. J. Styles, F. Lisi, C. J. Coghlan, C. J. Doonan, A. J. Hill, G. Brusatin and P. Falcaro, *Chem. Mater.*, 2015, **27**, 690–699.
21 J. Reboul, S. Furukawa, N. Horike, M. Tsotsalas, K. Hirai, H. Uehara, M. Kondo, N. Louvain, O. Sakata and S. Kitagawa, *Nat. Mater.*, 2012, **11**, 717–723.
22 N. Kornienko, Y. Zhao, C. S. Kley, C. Zhu, D. Kim, S. Lin, C. J. Chang, O. M. Yaghi and P. Yang, *J. Am. Chem. Soc.*, 2015, **137**, 14129–14135.
23 Z. Dai, S. Pradeep, J. Zhu, W. Xie, H. F. Barton, Y. Si, B. Ding, J. Yu and G. N. Parsons, *Adv. Mater. Interfaces*, 2021, **8**, 2101178.
24 L. Shao, F. Fan, X. Dai, H. Fu, W. Li, W. Qi, F.-B. Meng and Y. Fu, *Chem. Mater.*, 2022, **34**, 5356–5365.
25 H.-L. Wu, R. Sato, A. Yamaguchi, M. Kimura, M. Haruta, H. Kurata and T. Teranishi, *Science*, 2016, **351**, 1306–1310.
26 M. Leskelä and M. Ritala, *Angew. Chem., Int. Ed.*, 2003, **42**, 5548–5554.
27 A. J. M. Mackus, A. A. Bol and W. M. M. Kessels, *Nanoscale*, 2014, **6**, 10941–10960.
28 H. F. Barton, A. K. Davis and G. N. Parsons, *ACS Appl. Mater. Interfaces*, 2020, **12**, 14690–14701.
29 B. Gikonyo, F. Liu, S. Hawila, A. Demessence, H. G. Baldovi, S. Navalón, C. Marichy and A. Fateeva, *Molecules*, 2023, **28**, 5876.
30 A. Putnis, *Rev. Mineral. Geochem.*, 2009, **70**, 87–124.
31 S. Muralidharan and R. G. Hayes, *J. Chem. Phys.*, 1979, **71**, 2970–2974.
32 C. A. Schneider, W. S. Rasband and K. W. Eliceiri, *Nat. Methods*, 2012, **9**, 671–675.
33 N. Fairley, V. Fernandez, M. Richard-Plouet, C. Guillot-Deudon, J. Walton, E. Smith, D. Flahaut, M. Greiner, M. Biesinger, S. Tougaard, D. Morgan and J. Baltrusaitis, *Appl. Surf. Sci. Adv.*, 2021, **5**, 100112.
34 A. Fateeva, P. A. Chater, C. P. Ireland, A. A. Tahir, Y. Z. Khimyak, P. V. Wiper, J. R. Darwent and M. J. Rosseinsky, *Angew. Chem., Int. Ed.*, 2012, **51**, 7440–7444.